RADIO SCIENCE, VOL. 40, RS5S09, doi:10.1029/2004RS003135, 2005

Spatial filtering of interfering signals at the initial Low Frequency Array (LOFAR) phased array test station

A. J. Boonstra

Research and Development Department, Netherlands Foundation for Research in Astronomy, Dwingeloo, Netherlands

S. van der Tol

Department of Electrical Engineering, Delft University of Technology, Delft, Netherlands

Received 26 July 2004; revised 28 November 2004; accepted 2 March 2005; published 10 August 2005.

[1] The Low Frequency Array (LOFAR) is a radio telescope currently being designed. Its targeted observational frequency window lies in the range of 10–250 MHz. In frequency bands in which there is interference, the sensitivity of LOFAR can be enhanced by interference mitigation techniques. In this paper we demonstrate spatial filtering capabilities at the LOFAR initial test station (ITS) and relate it to the LOFAR radio frequency interference mitigation strategy. We show that in frequency ranges which are occupied with moderate-intensity man-made radio signals, the strongest observed astronomical sky sources can be recovered by spatial filtering. We also show that under certain conditions, intermodulation products of point-like interfering sources remain point sources. This means that intermodulation product filtering can be done in the same way as for "direct" interference. We further discuss some of the ITS system properties such as cross-talk and sky noise limited observations. Finally, we demonstrate the use of several beam former types for ITS.

Citation: Boonstra, A. J., and S. van der Tol (2005), Spatial filtering of interfering signals at the initial Low Frequency Array (LOFAR) phased array test station, *Radio Sci.*, *40*, RS5S09, doi:10.1029/2004RS003135.

1. Introduction

1.1. Low Frequency Array Interference Mitigation

[2] The Low Frequency Array (LOFAR) is a next generation radio telescope which is currently being designed and which will be located in the Netherlands. LOFAR [*Bregman*, 2000] is an aperture array telescope [*Thompson et al.*, 1986; *Raimond and Genee*, 1996] and will consist of order 100 telescopes (stations), spread in spirals over an area of about 360 km, as well as in a more densely occupied central core. The observational frequency window will lie in the 10–250 MHz range. Each of the stations will consist of order 100 phased array antennae. These antennae are sky noise limited, and are combined in such a way that station beams can be formed for each of the desired station observing directions or pointings. The preliminary LOFAR design defines multiple beam capabilities, (noncontiguous) 4 MHz wide bands, and a frequency resolution of 1 kHz. The LOFAR initial operations phase is scheduled to start in 2006; the target date to have LOFAR fully operational is 2008.

[3] For testing and demonstration purposes, several prototype stations are defined. One of these demonstrators is the initial test station (ITS). It is a full-scale prototype of a LOFAR station, and it became operational in December 2003. ITS consists of 60 sky noise limited dipoles, configured in a five-armed spiral, connected to a digital receiver back end. ITS operates in the frequency band 10–40 MHz, and the observed signals are directly digitized without the use of mixers. The data can be stored either as time series or as covariance matrices.

[4] In spectrum bands which are occupied with man-made radio signals with moderate signal powers, the unwanted man-made radio signals can be suppressed by applying filtering techniques. In this paper we demonstrate spatial filtering capabilities at the LOFAR ITS test station, and relate it to the LOFAR radio frequency interference (RFI) mitigation strategy [*Boonstra*, 2002]. We show the effect of these spatial filters by applying

0048-6604/05/2004RS003135$11.00

them to antenna covariance matrices, and by applying different beam-forming scenarios. We show that for moderate-intensity interferers (electric field strength $\leq$ 0 dBμVm^{-1}), the strongest observed astronomical sky sources can be recovered by spatial filtering. We also show that, under certain conditions, intermodulation products of point-like interfering sources remain point sources. This means that intermodulation product filtering can be done in the same way as for "direct" interference. We further discuss some of the ITS system properties such as cross talk and sky noise limited observations. Finally, we demonstrate the use of several beam former types for ITS.

1.2. Notation

[5] In this paper, scalars are denoted by nonbold lowercase and uppercase letters. Vectors are represented by bold lowercase letters, and matrices by uppercase bold letters. The hermitian conjugate transpose is denoted by $(.)^H$, the transpose operator by $(.)^t$, the expected value by $\mathcal{E}\{.\}$, and the estimated values by $\widehat{(.)}$. The element-wise multiplication (Hadamard) matrix operator is denoted by $\odot$. For a vector $\mathbf{a} = (a_1, \cdots, a_p)^t$, $e^{\mathbf{a}}$ is defined by $e^{\mathbf{a}} = (e^{a_1}, \cdots, e^{a_p})^t$. $\mathbf{I}$ represents the identity matrix, $\mathbf{A}^{-1}$ denotes the matrix inverse of $\mathbf{A}$, and $\mathbf{A}^{\frac{1}{2}}$ denotes the matrix $\mathbf{B}$ such that $\mathbf{B}^2 = \mathbf{A}$. Finally, $\jmath = \sqrt{-1}$, $\mathbf{0}$ is the null matrix, the complex conjugate is denoted by $\overline{(.)}$, and diag($\mathbf{a}$) converts the vector $\mathbf{a}$ to a diagonal matrix with $\mathbf{a}$ on the main diagonal.

2. LOFAR Interference Mitigation Strategy

[6] LOFAR will operate in bands where other spectrum users are active, and in which interference may occur. However, it is expected that the sensitivity of LOFAR can be enhanced by applying filtering and interference mitigation techniques. In this way, parts of the bands occupied with moderate-intensity man-made radio signals, can be recovered for astronomical observations. A description and results of some of the interference mitigation techniques applied in radio astronomy can be found in work by *Briggs et al.* [2000], *Ellingson et al.* [2001], *Leshem and van der Veen*, [2000], *Leshem et al.* [2000], *Fridman and Baan* [2001], and *Barnbaum and Bradley* [1998].

2.1. Spectral Occupancy and LOFAR Sensitivity

[7] LOFAR will be one of the first radio telescopes in which RFI mitigation techniques will form an integral part of the system design. For several reasons, it was decided to equip LOFAR with relatively simple RFI mitigation techniques. In future phases of LOFAR, these techniques may be extended. A first constraint on complexity is that the computing power required for interference mitigation should be an order of magnitude less than what is required for the astronomical signal processing. Only in special cases is spending a major fraction of the computing resources on RFI mitigation acceptable. A second reason for relatively simple techniques is that the calibration of LOFAR [*Noordam*, 2002, 2004] requires stable station beams. Only slowly varying (sidelobe) gains are allowed, otherwise the calibration process will not converge. For this reason, at station level, only spatial filters with fixed or slowly varying nulls are considered, as fast interference tracking would change the station beams too rapidly. A third reason is that interference mitigation is a relatively new field for radio astronomy, and that the effects of interference mitigation related distortions are not in all cases quantified.

[8] The use of the radio spectrum in terms of signal power and time-frequency occupancy is roughly known from allocation tables and from monitoring observations. In order to estimate the required attenuation levels, the observed spectrum power needs to be related to the LOFAR sensitivity. One of the key parameters of the LOFAR aperture synthesis mode is that LOFAR will be sky noise dominated and its desired ultimate sensitivity will be a factor eight better than the thermal sky noise in a four hour full synthesis observation with order 100 stations. *Kollen* [2004] specified a sensitivity of 2 mJy (1 Jy = 10^{-26} W m^2 Hz^{-1}) at 10 MHz down to 0.03 mJy at 240 MHz for 1 hour integration over 4 MHz bandwidth, which corresponds to a 1 kHz bandwidth to 127 mJy at 10 MHz down to 2.1 mJy at 240 MHz. In order to achieve this sensitivity and the required dynamic range, it is estimated that we need 4 MHz wide frequency bands for which we can recover 80% bandwidth. Here it is assumed that 20% bandwidth loss due to RFI does not lead to a dramatic decrease in sensitivity of the instrument as a whole. It is also assumed that in the 80% cleanest frequency bins within a 4 MHz band the RFI at station level is either at a 1–3 (station) sky noise sigma level, or can be reduced to this level by RFI mitigation techniques. The rationale of this is explained below.

2.2. Power Density Flux Levels

[9] The calibration capabilities of LOFAR [*Noordam*, 2002] include the removal of strong sky sources such as Cas.A from the observed (uvw) data sets and images. This suggests that the remaining RFI can be removed in the same way as astronomical sources are removed, assuming that RFI sources can be suppressed to levels comparable to the level of Cas.A. The LOFAR RFI strategy is based on this assumption which is illustrated in Figure 1. The vertical scale represents radio wave flux levels and sensitivities in Jy. The curve "antenna sky

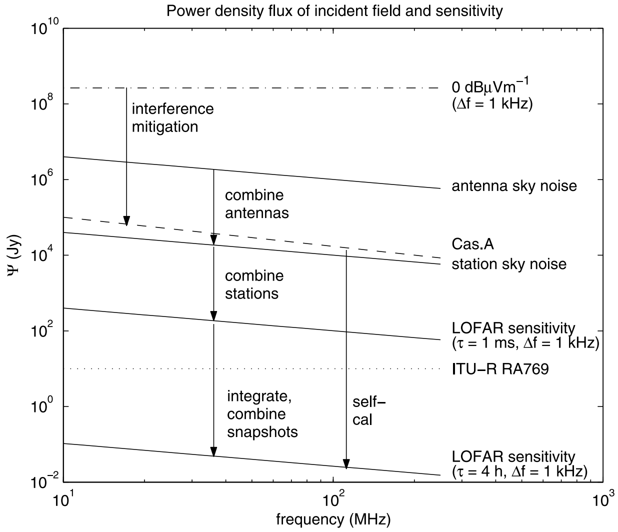

Figure 1. LOFAR sensitivity levels.

noise" shows the sky noise flux Ψ as a function of frequency, as would be observed with a single polarization LOFAR antenna dipole. It is based on the sky temperature, given by the approximate formula [*Bregman*, 2000; *Kraus*, 1986]

$$T_{sky} \approx T_{so}\lambda^{2.55}\ (K) \tag{1}$$

and on a formula [*Kraus*, 1986; *Rohlfs*, 1990] relating the sky temperature T_{sky} to the flux density Ψ

$$\Psi = 10^{26}\frac{2k}{\lambda^2}T_{sky}\Omega\ (Jy) \tag{2}$$

Here Ω is the antenna solid angle (assumed to be 4 Sr), k the Boltzmann constant, and T_{so} is 60 ± 20 K for angular distances to the galactic plane larger that 10°.

[10] The dash-dotted curve in Figure 1 denotes a transmitter or interference flux level, and corresponds to a free space field strength of 0 dBμVm^{-1}, assuming that the radio signal impinging on LOFAR is smeared out over a 1 kHz frequency channel width. At the LOFAR central core site in the Netherlands (above 30 MHz and outside the FM bands) nearly all transmitters and interferers have observed powers less than 40 dBμVm^{-1}. This was measured in a monitoring campaign; a large fraction of these transmitters even have observed powers below 0 dBμVm^{-1}.

[11] In a station, (order) 100 antennae are combined in a phased array to form one or more beam(s). This means that the RMS noise level at the beam output is decreased by 20 dB and becomes approximately equal to the noise power of Cas.A, one of the strongest sky sources. The RMS noise level at the beam output is represented by the curve "station sky noise" in Figure 1. It lies a few dBs below the "Cas.A" flux curve.

[12] In Figure 1, "LOFAR sensitivity" curves are drawn, both for 1 kHz bandwidth and for a synthesis array of (order) 100 stations. The two curves differ in integration time: 1 ms for the upper curve, and 4 h integration time for the bottom curve. Between the two LOFAR sensitivity curves, the ('mean') ITU-R RA769 emission criterion [*International Telecommunication Union*, 2003] is given, which roughly states the RFI level at which the error in determining the signal power exceeds 10% for an integration time of 2000 s.

2.3. LOFAR RFI Strategy

[13] The LOFAR RFI mitigation strategy is based on three steps. The first step in the strategy is choosing the optimum location for the LOFAR (order 200 kHz) subbands. Some of the 1 kHz bins in the 200 KHz bands may be affected by interference. In some cases, for example when a slight reduction of sensitivity is acceptable, these channels can be discarded, otherwise RFI mitigation measures need to be applied.

[14] The second step is reducing the RFI levels by RFI mitigation down to Cas.A power flux levels. These interference mitigation measures can be applied at station level before or after beam forming, or be applied at a central level, before or after correlation. Where this is optimally done in the signal chain is determined by various factors: the number of beam data bits, the data transport load, the number of correlator input bits, the linearity of the RFI Mitigation methods, etcetera. For LOFAR it was decided to apply only fixed or very slowly time-varying spatial nulls at station level. Fast changing interferer nulling directions would lead to fast changes in the (sidelobe) gains and this would hamper the calibration. Flagging or excising can best be done at a central level because interference often is localized. This means that interference may be present in one or a few stations, but not visible in an interferometer output. Flagging or excising at station level therefore often would remove too much data. The interference mitigation measures in the second step will be applied at timescales up to 10 s.

[15] Step three is the reduction of interference from 'Cas.A' level down to sky image noise levels. This step is closely related to the map making process and involves long integration times. Removing (stationary) interferers should not be too different from removing sources such as Cas.A. In addition to Selfcal and Clean, other methods could be used [*Leshem and van der Veen*, 2000; *Noordam*, 2004]. Long-term and short-term stationarity issues as well as estimation

biases [*Leshem et al.*, 2000; *Raza et al.*, 2002; *van der Tol and van der Veen*, 2004] are relevant here and require careful consideration.

[16] Two additional effects help reduce the observed interference. The first is spectral dilution. Suppose that in a LOFAR band a single narrowband RFI source is present. The energy of this RFI source is diluted by averaging all N_f frequency channels in the band. The noise power decreases with $\sqrt{N_f}$, whereas the RFI power decreases with N. This leads to a spectral dilution factor which scales with $\sqrt{N_f}$. For wideband signals such as CDMA (Code Division Multiple Access, a signal coding scheme), this obviously does not apply.

[17] A second effect which reduces interference is spatial dilution. In the aperture synthesis mode, snapshot images are made, and are integrated to form the integrated map. Sky sources move with respect to the baseline vectors during an observation. The interferers on the other hand do not move, or move differently. This means that in the integration process the sky sources remain at the same sky positions and are 'added'. The RFI sources move with respect to the sky and are therefore 'diluted'. The dilution for an RFI point source is comparable to the dilution of a narrowband signal due to frequency averaging: the system noise decreases with the square root of the number of snapshots whereas the RFI is reduced (as it moves around the map) by the number of snapshots. This means that if a point source is reduced to the station noise level, it will be reduced to below the integrated noise level by further integration (snapshot averaging). The spatial dilution is the two-dimensional variant of fringe rotation, observed in interferometers.

[18] On the basis of the analysis above and on initial observations with ITS, it seems feasible that the station sky noise level can be reached for certain frequency ranges, even in densely populated regions such as the Netherlands. With the help of Selfcal and Clean type approaches, the remaining RFI can be processed analogously to sources like Cas.A, and be further reduced to levels at or below the integrated sky noise.

3. Data Model

3.1. Received Data Model and Covariance Model

[19] In this section a single polarization point source telescope signal model is described [*Leshem et al.*, 2000]. This model includes a description of astronomical sources, additive interfering signals and noise. Assume that there are p telescope antennae, and suppose that the antenna signals $x_i(t)$ are composed of q_s astronomical source signals, q_r interfering sources, and noise. Let the telescope output signals $x_i(t)$ be stacked in a vector $\mathbf{x}(t)$

$$\mathbf{x}(t) = \left(x_1(t), x_2(t), \cdots, x_p(t)\right)^t \tag{3}$$

[20] Further let $\mathbf{x}^s_\ell(t)$ be the telescope array output signal corresponding to the ℓth astronomical source in the direction $\mathbf{s}_\ell$, let $\mathbf{x}^r_k(t)$ be the telescope array output signal corresponding to the kth interfering source in the direction $\mathbf{s}^r_k$, and let $\mathbf{x}^n(t)$ be the noise vector. The resulting array output signal then can be expressed by

$$\mathbf{x}(t) = \sum_{\ell=1}^{q_s} \mathbf{x}^s_\ell(t) + \sum_{k=1}^{q_r} \mathbf{x}^r_k(t) + \mathbf{x}^n(t) \tag{4}$$

[21] The noise $\mathbf{x}^n(t)$ is independent identically distributed (i.i.d.) Gaussian noise, so it is uncorrelated between the array elements, or in other words spatially white at the aperture plane. The astronomical source signals also are assumed to be identically distributed Gaussian noise signals. The sources are assumed to be independent, or in other words spatially white at the celestial sphere.

[22] For the LOFAR ITS telescope experiments, we assume that the narrowband interferer model [*Leshem et al.*, 2000; *Whalen*, 1971] holds. This means that for narrowband signals with bandwidth Δf, the condition

$$\Delta f \ll \frac{1}{2\pi\tau} \tag{5}$$

is valid, where τ denotes the geometrical signal time delay differences between the antenna elements. This condition implies that geometric time delay differences can be represented by phase shifts. For practical reasons, the frequency resolution for the observations discussed in this paper is 10 kHz, although the frequency resolution of LOFAR will be of the order of 1 kHz. The maximum geometric time delay across the array τ, is determined by the array size (200 m) and observation direction.

[23] Assume that there is an interferer with index k, with signal $y^r_k(t)$. Because the narrowband condition holds, the telescope output signal $\mathbf{x}^r_k(t)$ can be written in terms of the array response vector $\mathbf{a}^r_k$. Let the array response vector $\mathbf{a}^r_k$ be defined by

$$\mathbf{a}^r_k = \begin{pmatrix} a^r_1 e^{2\pi \jmath \frac{1}{\lambda}\left(\mathbf{b}_{10}\mathbf{s}^r_k\right)} \\ \vdots \\ a^r_p e^{2\pi \jmath \frac{1}{\lambda}\left(\mathbf{b}_{p0}\mathbf{s}^r_k\right)} \end{pmatrix} \tag{6}$$

where $\mathbf{b}_{i0}$ is the location of the ith antenna with respect to an arbitrary reference location, λ the wavelength of the impinging signal, and a_i^r are the antenna gains in the direction $\mathbf{s}_k^r$. This yields

$$\mathbf{x}_k^r(t) = \mathbf{a}_k^r y_k^r(t) \tag{7}$$

Let the antenna directional gain vector $\mathbf{a}_k^{rg}$ be defined by $\mathbf{a}_k^{rg} = (a_1^r, \cdots, a_p^r)^t$, and define $\mathcal{R} = (\mathbf{b}_{10}, \cdots, \mathbf{b}_{p0})^t$, then $\mathbf{a}_k^r$ can be compactly written as

$$\mathbf{a}_k^r = \mathbf{a}_k^{rg} \odot e^{\frac{2\pi}{\lambda} j \mathcal{R} \mathbf{s}_k^r} \tag{8}$$

Here the vector $e^{\frac{2\pi}{\lambda} j \mathcal{R} \mathbf{s}_k^r}$ represents the geometrical delay (phase) vector for the telescope antenna locations $\mathcal{R}$ and the source direction $\mathbf{s}_k^r$.

[24] Assume there are q_r interferers, and define $\mathbf{x}^r(t)$ by $\mathbf{x}^r(t) = \Sigma_k\, \mathbf{x}_k^r(t)$, which also can be written as

$$\mathbf{x}^r(t) = \sum_{k=1}^{q_r} \mathbf{a}_k^r y_k^r(t) \tag{9}$$

[25] The interferer signal power σ_k^2 is given by $\mathcal{E}\{y_k^r(t)\overline{y_k^r(t)}\} = \sigma_k^2$, which leads to the following expression for the interference array covariance matrix $\mathbf{R}_r$, dropping the time index t for $\mathbf{R}_r$:

$$\mathbf{R}_r = \mathcal{E}\left\{x^r(t)x^r(t)^H\right\} = \sum_{k=1}^{q_r} \sigma_k^2 \mathbf{a}_k^r \left(\mathbf{a}_k^r\right)^H \tag{10}$$

[26] The array response vector and the covariance matrix $\mathbf{R}_s$ for astronomical sources can be expressed in a similar way. Concerning the system noise, it can be represented by a diagonal noise matrix $\mathbf{D}$, and is given by

$$\mathbf{D} = \mathcal{E}\left\{\mathbf{x}^n(t)\mathbf{x}^n(t)^H\right\} = \operatorname{diag}\left(\sigma_1^2, \cdots, \sigma_p^2\right) \tag{11}$$

where the σ_i^2 is the noise power of the ith antenna without source or interferer contributions.

[27] The covariance matrix

$$\mathbf{R} = \mathcal{E}\left\{\mathbf{x}(t)\mathbf{x}(t)^H\right\} \tag{12}$$

can be expressed as

$$\begin{aligned}\mathbf{R} &= \mathbf{R}_r + \mathbf{R}_s + \mathbf{D} \\ &= \sum_{k=1}^{q_r} \sigma_k^2 \mathbf{a}_k^r \left(\mathbf{a}_k^r\right)^H + \sum_{\ell=1}^{q_s} \sigma_\ell^2 \mathbf{a}_\ell^s \left(\mathbf{a}_\ell^s\right)^H + \mathbf{D}\end{aligned} \tag{13}$$

[28] Let $\mathbf{A}_r$ be defined by stacking the array response vectors for the interferers in a matrix

$$\mathbf{A}_r = \left[\mathbf{a}_1^r, \cdots \mathbf{a}_{q_r}^r\right] \tag{14}$$

and stack the interfering source powers in a diagonal matrix $\mathbf{B}_r$. For the astronomical sources the same definitions for $\mathbf{A}_s$ and $\mathbf{B}_s$ can be made. Using these definitions, the covariance matrix $\mathbf{R}$ can be expressed in a more compact form:

$$\mathbf{R} = \mathbf{A}_r \mathbf{B}_r \mathbf{A}_r^H + \mathbf{A}_s \mathbf{B}_s \mathbf{A}_s^H + \mathbf{D} \tag{15}$$

3.2. Imaging and Beam Forming

[29] Traditionally [*Perley et al.*, 1994], the synthesized sky images are generated by fourier transforming the correlation data, here represented by the covariance matrix $\mathbf{R}$. For the ITS station, the observed snapshots contain only a fairly limited number of spatial sample points. This implies that making sky images with the ITS station using beam forming is more practical than using spatial fourier transforms. Therefore the beam forming approach, used for ITS imaging, is discussed next.

[30] Assume that the complex gain of the array antenna elements can be adjusted by a multiplicative complex weight number w_i for each of the antenna elements i. Given the array output signal vector $\mathbf{x}(t)$ and a weight vector for the array $\mathbf{w} = (w_1, \cdots, w_p)^t$, then the weighted-summed array output signal $y(t)$ is given by

$$y(t) = \mathbf{w}^H \mathbf{x}(t) \tag{16}$$

The beam former output power P is then given by

$$P = \mathcal{E}\left\{y(t)y(t)^H\right\} = \mathbf{w}^H \mathcal{E}\left\{x(t)x(t)^H\right\}\mathbf{w} = \mathbf{w}^H \mathbf{R} \mathbf{w} \tag{17}$$

[31] For a classical or capon beam former we can define the weight vector, in terms of sky direction cosine coordinates (l,m):

$$\mathbf{w}^H(l,m) = \mathbf{a}^H(l,m) \tag{18}$$

where $\mathbf{a}(l, m)$ is the array response to signals from direction (l, m). The classical beam former is equivalent to direct fourier transforming or taking the fourier transform of all u,v data points without weighting. The sidelobe pattern of this beam former is shown in Figure 2.

4. Measurement Results

4.1. ITS Test Station

[32] The LOFAR ITS test station is located in the northeast of the Netherlands. It is a sky noise limited antenna array station consisting of $p = 60$ linearly polarized antennae which are grouped in five spiral arms. Each of the arms contain 12 single polarization inverted-

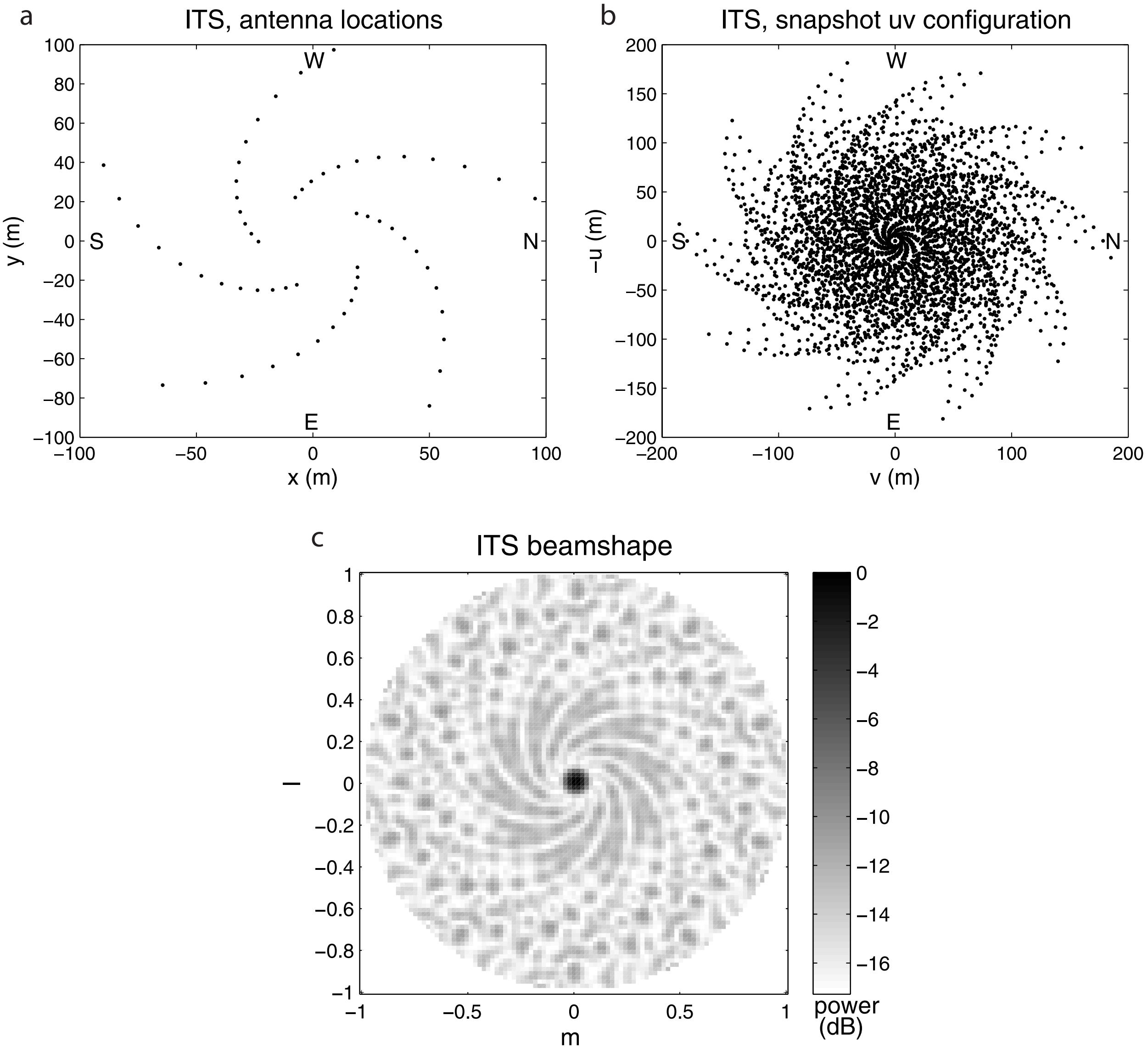

Figure 2. (a) LOFAR station ITS antenna configuration, (b) station snapshot (u, v) coverage, and (c) station beam shape when the beam is aimed in the zenith direction. The beam shape actually is the response to the entire hemisphere of sky (down to the horizon).

v dipoles with a resonance frequency of 34 MHz as can be seen in Figure 3. The dipoles are oriented in an east-west direction. The shortest antenna distance is 5 m, which corresponds to $\frac{1}{2}\lambda$ at 30 MHz. The diameter of the station is 200 m. The geometrical layout of the antenna locations is given in Figure 2a. A snapshot correlation measurement combines each of the antennae with all the others, yielding p^2 interferometer products. Each interferometer product corresponds to a certain telescope distance and direction, called baseline. Figure 2 (top right) shows the snapshot baseline configuration in a righthanded coordinate (u, v, w) system. Figure 2b shows the way in which the aperture is spatially sampled. Combining snapshot images will gradually fill the open spaces because the earth rotation changes the relative antenna positions with respect to the sky. Figure 2c shows the phased array beam shape at 30 MHz for the zenith direction. The beam width at this frequency is

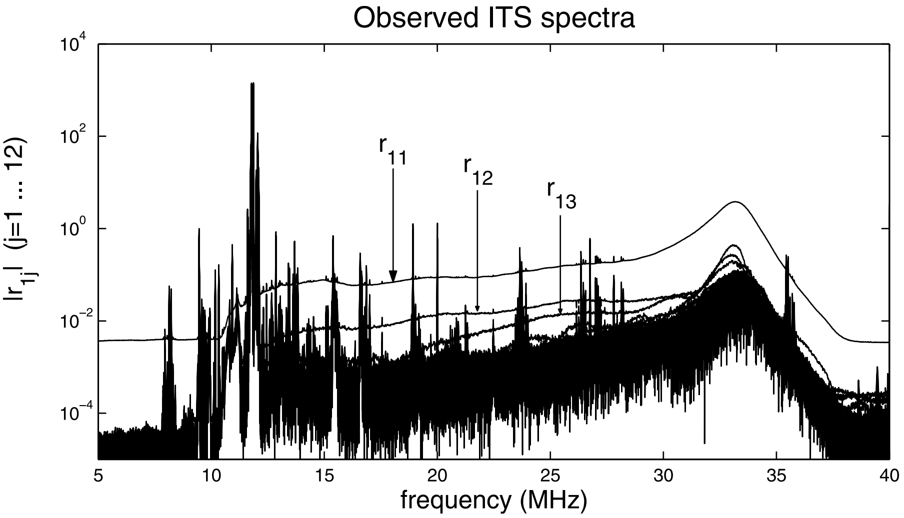

Figure 3. Nighttime ITS test station spectra of interferometers r_{1j}, with $j = 1 \cdots 12$ and $\Delta f =$ 9.77 kHz.

5.5°. The coordinates are direction cosines (l,m). The north is defined in the positive m direction, the east in the positive l direction.

[33] The antenna outputs are connected to low-noise amplifiers, filtered by a 10–35 MHz filter, and digitized with a sampling frequency of 80 MHz. For the experiments described in this paper, a 8192 sample length, Hanning tapered, FFT was used. This yielded a frequency resolution of 9.77 kHz. The spectra were correlated and integrated to 6.7 s, yielding a 60 × 60 covariance matrix for each of the 4096 frequency bins. Figure 3 shows 12 observed interferometer spectra, of the inner antenna of one of the arms, correlated with all antennae in the same arm. Disconnecting an antenna and attaching a matched load instead, reduces the observed autocorrelation power $\mathbf{R}_{11}$ by ≈75%, indicating that the sky noise is the largest contributor to the system noise. Further proof is given by *Wijnholds et al.* [2005], where it is shown that the noise in the observed snapshot images is dominated by the sky noise.

[34] Figure 3 also shows that the magnitudes of $\mathbf{R}_{12}$, $\mathbf{R}_{13}$, and $\mathbf{R}_{14}$ are higher than those of the longer baselines. This is caused by the astronomical extended sources in the sky, a well-known effect in aperture synthesis [*Kraus*, 1986; *Rohlfs*, 1990; *Perley et al.*, 1994]. As the antennae closest to the center of the ITS station ($\mathbf{b}_{10}$ and $\mathbf{b}_{20}$) are only at a $\frac{1}{2}\lambda$ distance at 30 MHz, there will be mutual coupling. This means that part of the sky and receiver noise current in an antenna is coupled to the other elements. In addition there could be electronic coupling between receiver boxes, cabling etcetera. Crosstalk would be best visible on the shortest antenna spacings, making it difficult to distinguish it from extended astronomical sources. Method of moment antenna simulations show however, that the crosstalk fraction of the dipole at 40 MHz is −20 dB, and decreases to −43 dB at 30 MHz and −65 dB at 20 MHz. This implies that the cross talk can be ignored for most data processing applications.

[35] The observed spectrum shows that a large fraction of the 15–35 MHz band is sky noise limited at night, so LOFAR observations could be carried out in those frequency slots. By day the spectrum is more densely occupied; an inventory of the occupancy statistics at ITS is currently being carried out. The spectrum shows harmonics and intermodulation products of strong transmitters at 12 MHz. These signals appear at 24 and 36 MHz. As will be shown in the next sections, these harmonics and intermodulation products can be suppressed in the same way as "ordinary" transmitters.

4.2. Spatial Filtering

[36] Spatial filtering is demonstrated by applying projection filters and subtraction filters to the observed covariance matrices $\widehat{\mathbf{R}}$. These matrices $\widehat{\mathbf{R}}$ are sample estimates of $\mathbf{R}$ and are constructed by

$$\widehat{\mathbf{R}} = \frac{1}{N} \sum_{n=1}^{N} \mathbf{x}_n \mathbf{x}_n^H \tag{19}$$

[37] Here $\mathbf{x}_n$ is the array signal output vector at time index n; this index replaces the time variable t in equation (4). We assume that model (15) is valid. As we are investigating the suppression of relatively strong

interferers, we assume that the interferer power σ_k^2 is much larger than the astronomical sources power σ_ℓ^2. We further assume that the noise power matrix **D** contains the spatially white sky noise which is dominant in strength. Now **D** is initially unknown but it can be estimated for example with factor analysis approaches [*Mardia et al.*, 1979; *Boonstra and van der Veen*, 2003a, 2003b]. Once **D** is estimated, the matrix $\widehat{\mathbf{R}}$ can be whitened, for example by premultiplying and postmultiplying it with $\widehat{\mathbf{D}}^{-\frac{1}{2}}$. The whitening process also affects $\widehat{\mathbf{R}}_s$, but this can be corrected after filtering. Consider now the following simplified whitened model

$$\mathbf{R} = \mathbf{A}_r\mathbf{B}_r\mathbf{A}_r^H + \mathbf{R}_s + \sigma_n^2\mathbf{I} \tag{20}$$

where we assume that the interferer power is dominant. This model will be used further to explain the working of the spatial filters.

4.2.1. Projection Filtering

[38] The covariance matrix **R** can be filtered using projection matrices [*Leshem et al.*, 2000]. As before, let $\mathbf{A}^r$ be a matrix containing the interferer array response vectors $\mathbf{a}_k^r$, and assume that $\mathbf{A}^r$ is known. Define the projection matrix **P** by

$$\mathbf{P} = \mathbf{I} - \mathbf{A}_r\left(\mathbf{A}_r^H\mathbf{A}_r\right)^{-1}\mathbf{A}_r^H \tag{21}$$

Because $\mathbf{P}\mathbf{A}_r = \mathbf{0}$, pre and post multiplying **R** with **P** yields for the filtered covariance matrix $\check{\mathbf{R}}_\perp$:

$$\check{\mathbf{R}}_\perp = \mathbf{P}\widehat{\mathbf{R}}\mathbf{P} \tag{22}$$

$$\mathcal{E}\{\check{\mathbf{R}}_\perp\} = \mathbf{P}\left(\mathbf{R}_s + \sigma_n^2\mathbf{I}\right)\mathbf{P} \tag{23}$$

The interference is removed, but the astronomical sources are distorted by the filter. This distortion can be removed by approaches such as described by *Leshem et al.* [2000], *Raza et al.* [2002], and *van der Tol and van der Veen* [2004], but it is beyond the scope of this paper to apply these techniques here.

4.2.2. Subtraction Filtering

[39] An alternative filtering method is interference subtraction. With known σ_n^2, $\mathbf{B}_r$, and $\mathbf{A}_r$, or their estimates, the contribution of the interferer can be reduced by subtracting it from the observed covariance matrix. Let $\check{\mathbf{R}}\_$ be the filtered covariance matrix, that is the observed covariance matrix with the estimated interference removed by subtraction, then:

$$\check{\mathbf{R}}_- = \widehat{\mathbf{R}} - \mathbf{A}_r\mathbf{B}_r\mathbf{A}_r^H \tag{24}$$

$$\mathcal{E}\{\check{\mathbf{R}}_-\} = \mathbf{R}_s + \sigma_n^2\mathbf{I} \tag{25}$$

4.2.3. Attenuation Limits and Subspace Analysis

[40] When the spatial signature of the interferers and its power is unknown, it can be estimated by an eigenanalysis of the sample covariance matrix $\widehat{\mathbf{R}}$. Because of limits in the estimation accuracies, both filter types will have estimation errors and may also be biased [*Leshem and van der Veen*, 2000]. In some case the bias can be corrected [*van der Tol and van der Veen*, 2004]. These estimation errors will not be discussed in detail here. Now we will briefly describe how to estimate the interferer parameters using a subspace analysis. The covariance matrix **R** can be written in terms of eigenvalues and eigenvectors as [*Leshem et al.*, 2000]

$$\mathbf{R} = \mathbf{U}\boldsymbol{\Lambda}\mathbf{U}^H \tag{26}$$

where **U** is a unitary matrix containing the eigenvectors, and $\boldsymbol{\Lambda}$ is a diagonal matrix containing the eigenvalues. Assuming that the astronomical contribution is so small it can be ignored, with the exception of the extended spatially white emission, the eigenvalue decomposition can be expressed as

$$\mathbf{R} = [\mathbf{U}_r\mathbf{U}_n]\begin{bmatrix} \boldsymbol{\Lambda}_r + \sigma_n^2\mathbf{I}_{q_r} & 0 \\ 0 & \sigma_n^2\mathbf{I}_{p-q_r} \end{bmatrix}\begin{bmatrix} \mathbf{U}_r^H \\ \mathbf{U}_n^H \end{bmatrix} \tag{27}$$

where $\mathbf{U}_r$ is a $p \times q_r$ matrix, containing the eigenvectors corresponding to the q_r eigenvalues in $\boldsymbol{\Lambda}_r$. $\mathbf{U}_n$ is a $p \times (p-q_r)$ matrix containing the eigenvectors, corresponding to the noise subspace. Given a matrix **R**, the signal subspace can be found by applying a singular value decomposition to **R**. Note that the signal subspace and the noise subspace span the entire space, $\mathbf{U} = [\mathbf{U}_r\mathbf{U}_n]$, and **U** is unitary: $\mathbf{U}\mathbf{U}^H = \mathbf{U}_s\mathbf{U}_s^H + \mathbf{U}_n\mathbf{U}_n^H = \mathbf{I}_p$. Without further knowledge, the best estimate of $\mathbf{A}_r$ is the dominant eigenspace $\mathbf{U}_r$ of $\widehat{\mathbf{R}}$, and likewise the best estimate of the interferer powers $\mathbf{B}_r$ is $\boldsymbol{\Lambda}_r$.

4.2.4. Experimental Results

[41] Figure 4 shows the eigenvalue structure of $\widehat{\mathbf{R}}$ of the nighttime observation discussed earlier. The eigenvalue decomposition was applied after a whitening step. The largest eigenvalue of the observed transmitter at 25.752 MHz lies 20 dB above the remaining eigenvalues. This means that the observed transmitter power lies 20 dB above the sky noise level, and that the transmitter occupies (for at least 99% of its power) only one dimension of the subspace of $\widehat{\mathbf{R}}$. Therefore we have chosen to base the spatial filters on one direction vector only, namely the one corresponding to the largest eigenvalue.

[42] Figure 5a, shows the results of the beam former scan over the entire sky of the data set of 26 February

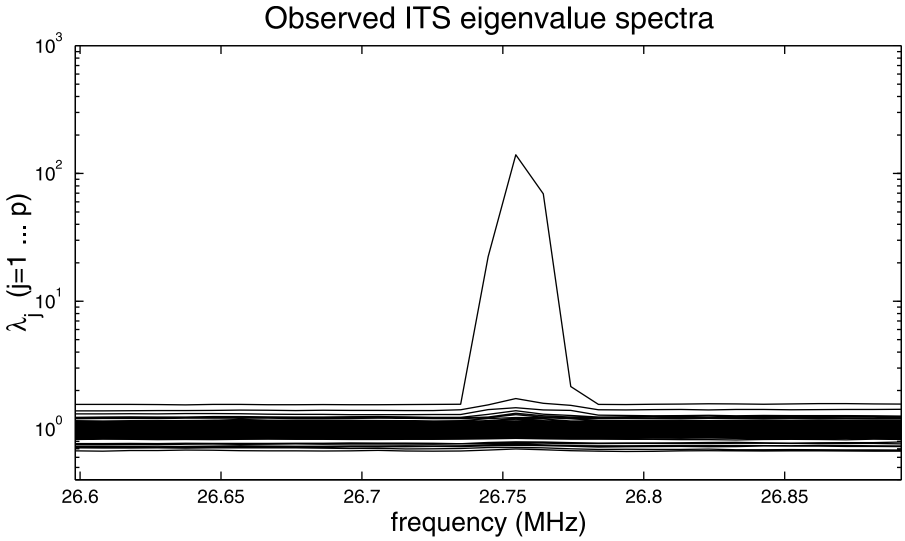

Figure 4. Eigenvalue distribution for N_{sam} = 131,000, Δt = 6.7 s, Δf = 9.77 kHz, measured on 26 February 2004.

2004, at 03:50 MET. The sky is shown at a single frequency bin at 26.89 MHz; no interference or transmitters were detected. The astronomical sources Cas.A (to the right of the image), and Cyg.A (near the top of the image) are clearly visible. An extended structure, the "north galactic spur" is just visible as a band from (m,l) = (−0.6, −0.2) to (m,l) = (−0.3, 0.9). Figure 5b is a sky image from the same data set, but now at 26.75 MHz in which a transmitter was detected. It is visible at the horizon at (l,m) = (0.45, −0.9). It is 20 dB above the noise (cf. Figure 4), and its sidelobes spread around the map and obscure the astronomical sources. In Figure 5c, the same map is shown, but now it is improved by applying a projection filter. In this experiment, the distortion correction, discussed earlier, was not applied. Clearly, sidelobe structure residuals of the uncorrected projection filter distort the map more than the subtraction filter which is shown in Figure 5d. This, however, does not imply that subtraction filters are better than projection filters, as the projection filter was uncorrected. The point here is that spatial filtering can attenuate a transmitter 20 to 30 dB above the sky noise to levels below the Cas.A flux level. At 18.92 MHz we showed (not displayed here), the same for a transmitter 30 dB above the sky noise level. The residual transmitter sidelobes were also suppressed to levels below Cas.A.

4.2.5. Detection of RFI Using Eigenvalue Decomposition

[43] As a further illustration of the relation between the eigenstructure of the observed covariance matrices and the number of detectable interfering sources, we show two examples in Figure 6. Figure 6a shows an eigenvalue distribution with one dominant largest eigenvalue and one dominant source in the accompanying map. Figure 6b shows three dominant eigenvalues and three interfering sources in the map.

4.3. Intermodulation Products

[44] The purpose of the following analysis is to show that intermodulation products appear as additional point sources in the map. The consequence of this is that these sources can be mitigated just like ordinary sources and that spatial dilution is also applicable for these sources.

[45] Intermodulation products are caused by nonlinearities in the receiver, often caused by high-power transmitter signals distorting the low-noise amplifier linearity. Assume that the transmitter signals are semi stationary. For a simple second-order model of the amplifier and given input signal $x(t)$, the output $y(t)$ is given by

$$y(t) = \beta_1 x(t) + \beta_2 x^2(t) \tag{28}$$

where β_1 and β_2 are two real parameters describing the (non)linearity behavior. Let us consider the scenario where the input consists of the sum of two cosines with different amplitude (α_1, α_2), frequency (f_1, f_2) and phase (θ_1, θ_2)

$$\begin{aligned} x(t) = {} & \alpha_1 \cos(2\pi f_1 t + \theta_1) \\ & + \alpha_2 \cos(2\pi f_2 t + \theta_2) \end{aligned} \tag{29}$$

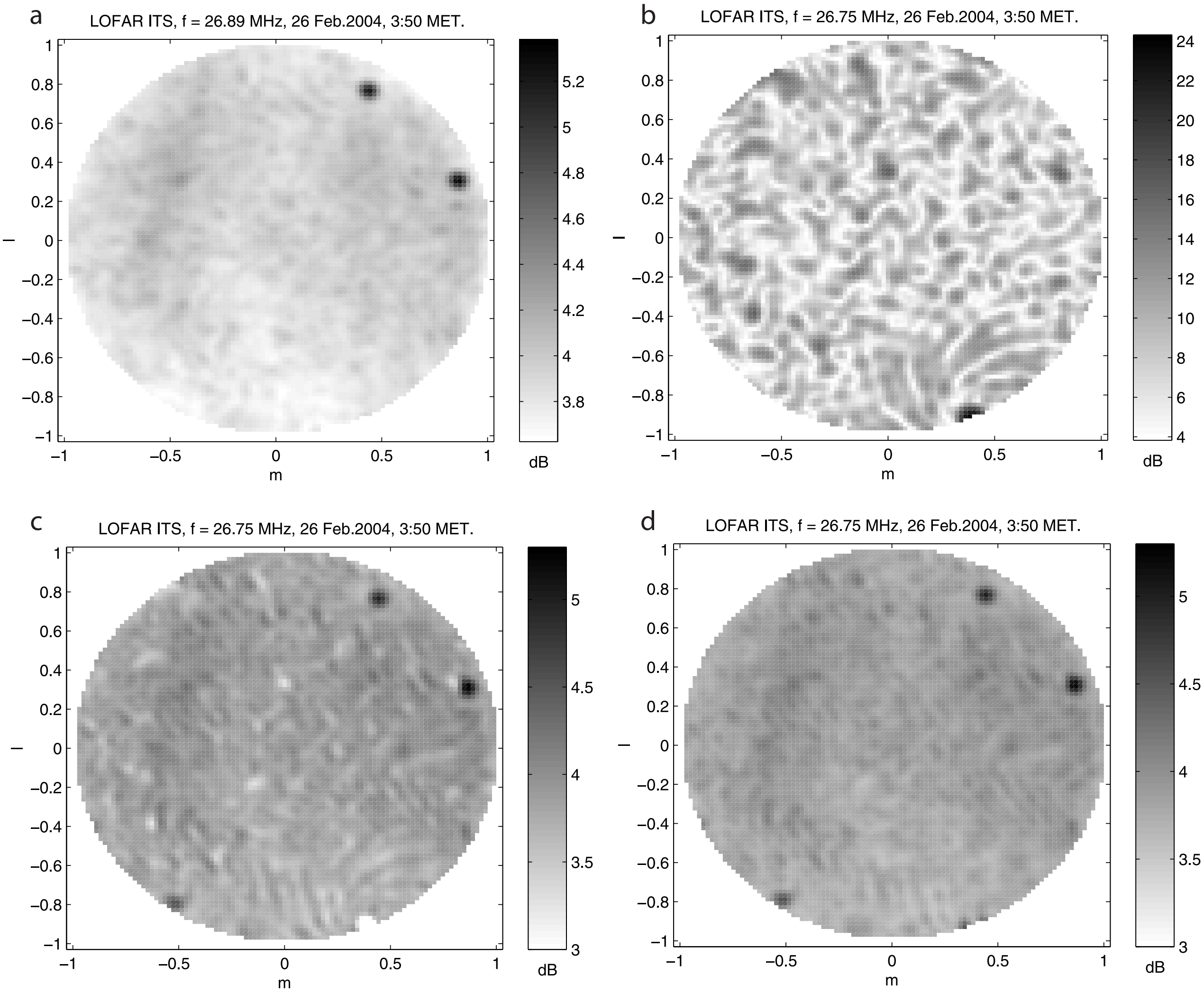

Figure 5. Spatial filtering at LOFAR ITS test station: (a) snapshot image without interference at 26.89 MHz, (b) snapshot image with a transmitter at 26.75 MHz, (c) image with transmission removed by spatial filtering using a projection filter, and (d) image with transmission removed by spatial filtering using a subtraction filter.

the output of the amplifier is then given by

$$\begin{aligned} y(t) = {} & \beta_1\alpha_1\cos(2\pi f_1 t + \theta_1) + \beta_1\alpha_2\cos(2\pi f_2 t + \theta_2) \\ & + \beta_2\alpha_1^2/2(1 + \cos(2\pi 2 f_1 t + 2\theta_1) \\ & + \beta_2\alpha_2^2/2(1 + \cos(2\pi 2 f_2 t + 2\theta_2) \\ & + \beta_2\alpha_1\alpha_2\cos(2\pi(f_1 + f_2) + \theta_1 + \theta_2) \\ & + \beta_2\alpha_1\alpha_2\cos(2\pi(f_1 - f_2) + \theta_1 - \theta_2) \end{aligned} \tag{30}$$

The first two terms are wanted, the last four are intermodulation products.

[46] Now consider two cosine signals impinging on an array of antennae. The sum of these two cosines can be modeled as

$$\begin{aligned} \mathbf{x}(t) = {} & \boldsymbol{\alpha}_1 \odot \cos(2\pi f_1 t\underline{1} + \boldsymbol{\theta}_1) \\ & + \boldsymbol{\alpha}_2 \odot \cos(2\pi f_2 t\underline{1} + \boldsymbol{\theta}_2) \end{aligned} \tag{31}$$

where $\boldsymbol{\alpha}_k$ is the vector containing the real signal amplitudes, and $\boldsymbol{\theta}_k$ is the antenna phase vector of the kth transmitter. The phase vector $\boldsymbol{\theta}_k$ can be expressed in terms of geometric telescope positions $\mathcal{R} = (\mathbf{b}_{10}, \cdots,$

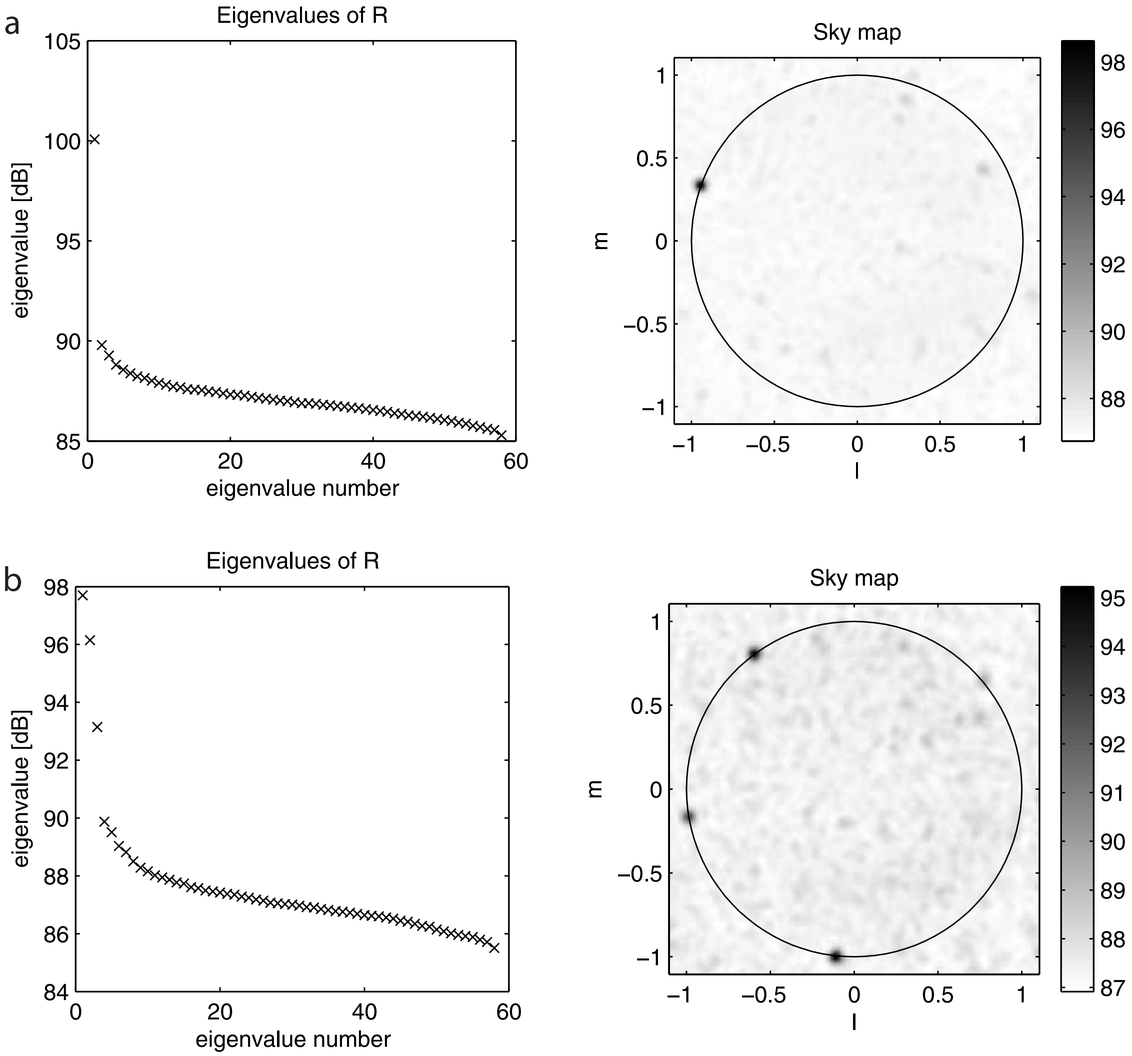

Figure 6. Eigenvalue decomposition of covariance matrices and celestial maps from the LOFAR initial test station. Shown are observations at (a) 27.800 and (b) 27.096 MHz. There is a clear correlation between the number of observed strong sources and the number of large eigenvalues.

$\mathbf{b}_{p0})^t$, wavelength λ_k and the source direction $\mathbf{s}_k$ of the kth transmitter

$$\theta_k = \frac{2\pi}{\lambda_k} \mathcal{R} \mathbf{s}_k \tag{32}$$

The transmitter source direction vector $\mathbf{s}_k$ is a unit norm vector.

$$\mathbf{s}_k \equiv \begin{bmatrix} l \\ m \\ n \end{bmatrix} \tag{33}$$

Table 1. Predicted Directions in (l,m) Coordinates of Transmitters and Their Intermodulation Products as They Will Appear in Celestial Maps

f	l	m
f_1	l_1	m_1
f_2	l_2	m_2
$2f_1$	l_1	m_1
$2f_2$	l_2	m_2
f_1+f_2	$\frac{\lambda_2 l_1 + \lambda_1 l_2}{\lambda_1 + \lambda_2}$	$\frac{\lambda_2 m_1 + \lambda_1 m_2}{\lambda_1 + \lambda_2}$
f_1-f_2	$\frac{\lambda_2 l_1 - \lambda_1 l_2}{\lambda_1 - \lambda_2}$	$\frac{\lambda_2 m_1 - \lambda_1 m_2}{\lambda_1 - \lambda_2}$

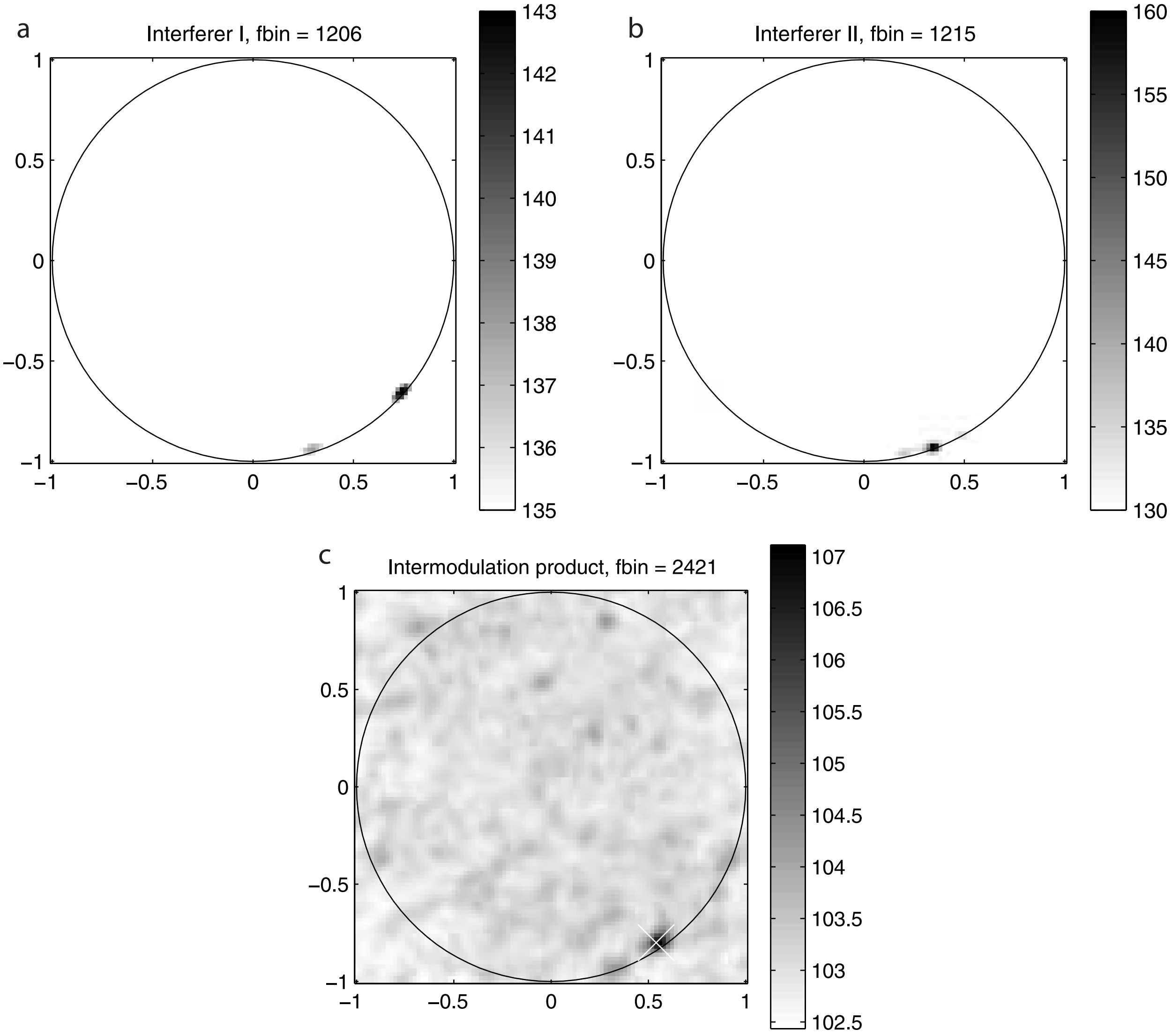

Figure 7. Two strong interfering point sources are visible at the horizon at (a) 11.77 and (b) 11.86 MHz. (c) The summed frequency intermodulation product is visible at a location in between the two "parent" sources. The intermodulation product is marked with a cross and remains a point source.

[47] To specify a location only two coordinates (l, m) are necessary, the third coordinate is chosen such that the vector unit norm. For a planar array in the x,y plane the z coordinate of the antenna positions is zero. All items of the third column of $\mathcal{R}$ are zero, which means that the phase $\boldsymbol{\theta}$ is independent of the third component of $\mathbf{s}_k$.

[48] The sum of two cosines with frequencies f_1 and f_2 at the input gives the sum of six cosines with frequencies f_1, f_2, $2f_1$ $2f_2$, $f_1 + f_2$ and $f_1 - f_2$. Let us consider the intermodulation response $\mathbf{y}_i(t)$ at $f_{12} = f_1 + f_2$ in more detail

$$\mathbf{y}_i(t) = \boldsymbol{\beta}_2 \odot \boldsymbol{\alpha}_1 \odot \boldsymbol{\alpha}_2 \odot \cos(2\pi(f_1 + f_2)t\mathbf{1} + \boldsymbol{\theta}_1 + \boldsymbol{\theta}_2) \tag{34}$$

where $\boldsymbol{\beta}_2$ is the vector containing the second-order nonlinearity parameters for each of the antennae.

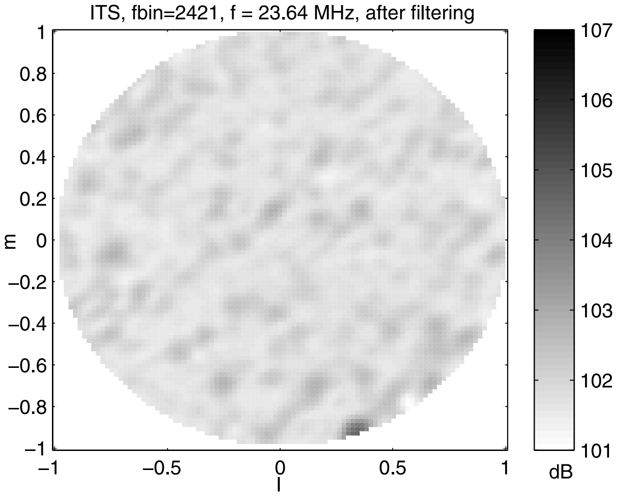

Figure 8. Sky map showing the effect of a rank-1 spatial projection filter on an intermodulation product. The intermodulation product, a point source, is suppressed by at least 10 dB.

The sum of the phases $\theta_1 + \theta_2$ can be expressed by

$$\begin{aligned}\theta_1 + \theta_2 &= \frac{2\pi}{\lambda_1}\mathcal{R}\mathbf{s}_1 + \frac{2\pi}{\lambda_2}\mathcal{R}\mathbf{s}_2 \\ &= 2\pi\mathcal{R}\left(\frac{\mathbf{s}_1}{\lambda 1} + \frac{\mathbf{s}_2}{\lambda 2}\right)\end{aligned} \tag{35}$$

[49] Suppose there exists a real source (i.e., not an intermodulation product) at frequency $f_{12} = f_1 + f_2$, or wavelength λ_{12}

$$\lambda_{12} = \frac{\lambda_1\lambda_2}{\lambda_1 + \lambda_2} \tag{36}$$

and suppose this source has a direction given by

$$\mathbf{s}_{12} = \frac{\lambda_2\mathbf{s}_1 + \lambda_1\mathbf{s}_2}{\lambda_1 + \lambda_1} \tag{37}$$

Then this source will have the following phases

$$\begin{aligned}\theta &= \frac{2\pi}{\lambda_{12}}\mathcal{R}\mathbf{s}_{12} \\ &= 2\pi\mathcal{R}\frac{\lambda_1 + \lambda_2}{\lambda_1\lambda_2}\frac{\lambda_2\mathbf{s}_1 + \lambda_1\mathbf{s}_2}{\lambda_1 + \lambda_1} \\ &= 2\pi\mathcal{R}\left(\frac{\mathbf{s}_1}{\lambda 1} + \frac{\mathbf{s}_2}{\lambda 2}\right)\end{aligned} \tag{38}$$

These phases are equal to the phases of the intermodulation product described earlier, which means that the intermodulation product will appear as a point source in the map in the weighted direction $\mathbf{s}_{12}$. The direction vector $\mathbf{s}_{12}$ is not unit norm, but there does exist a vector with the same (l, m) and a different n coordinate which is unit norm. Since for a planar array the phases do not depend on the n coordinate, a signal from this direction has the same phases as the intermodulation product. The absolute value of the spatial signature is different.

[50] So we can conclude that intermodulation products appear as additional sources in the image at predictable positions as given in Table 1. As the nonlinearity variation over the array differs from the antenna (sidelobe) gain variation over the array, in principle we can distinguish intermodulation products from real sources.

[51] Figure 7 shows an ITS observation with strong interferers at 11.77 MHz and 11.86 MHz. The intermodulation product consisting of the sum of the two signals appears exactly at the predicted location, indicated by the white cross. Figure 8 shows the same data set, but shown after application of a spatial projection filter. The intermodulation product clearly is removed by the rank-1 filter. What remains are nearby (multipath?) sources, which can be removed as well by increasing the rank or subspace of the projection filter.

4.4. Minimum Variance Distortionless Response and Robust Capon Beam Forming

[52] The weights of the classical beam former are independent of the data. The image quality can be improved by using a data-dependent beam former. Minimum variance distortionless response (MVDR) beam forming [*Madisetti and Williams*, 1998; *Van Trees*, 2002] gives a significant suppression of the sidelobes compared to classical beam forming. The MVDR beam former minimizes the output power under the constraint that the gain in the desired direction remains unity:

$$\mathbf{w}_{\mathrm{MVDR}}(l,m) = \arg\min_{\mathbf{w}} \mathbf{w}(l,m)^H\mathbf{R}\mathbf{w}(l,m) \tag{39}$$

with the constraint

$$\mathbf{w}_{\mathrm{MVDR}}(l,m)^H\mathbf{a}(l,m) = 1 \tag{40}$$

The solution to this equation can be found using Lagrange multipliers, and is given by

$$\mathbf{w}_{\mathrm{MVDR}}(l,m) = \frac{\mathbf{R}^{-1}\mathbf{a}(l,m)}{\mathbf{a}(l,m)^H\mathbf{R}^{-1}\mathbf{a}(l,m)} \tag{41}$$

The measured intensity is given by

$$I(l,m) = \frac{1}{\mathbf{a}(l,m)^H\mathbf{R}^{-1}\mathbf{a}(l,m)} \tag{42}$$

The MVDR beam former is known to be sensitive to array calibration errors, leading to errors in the beam

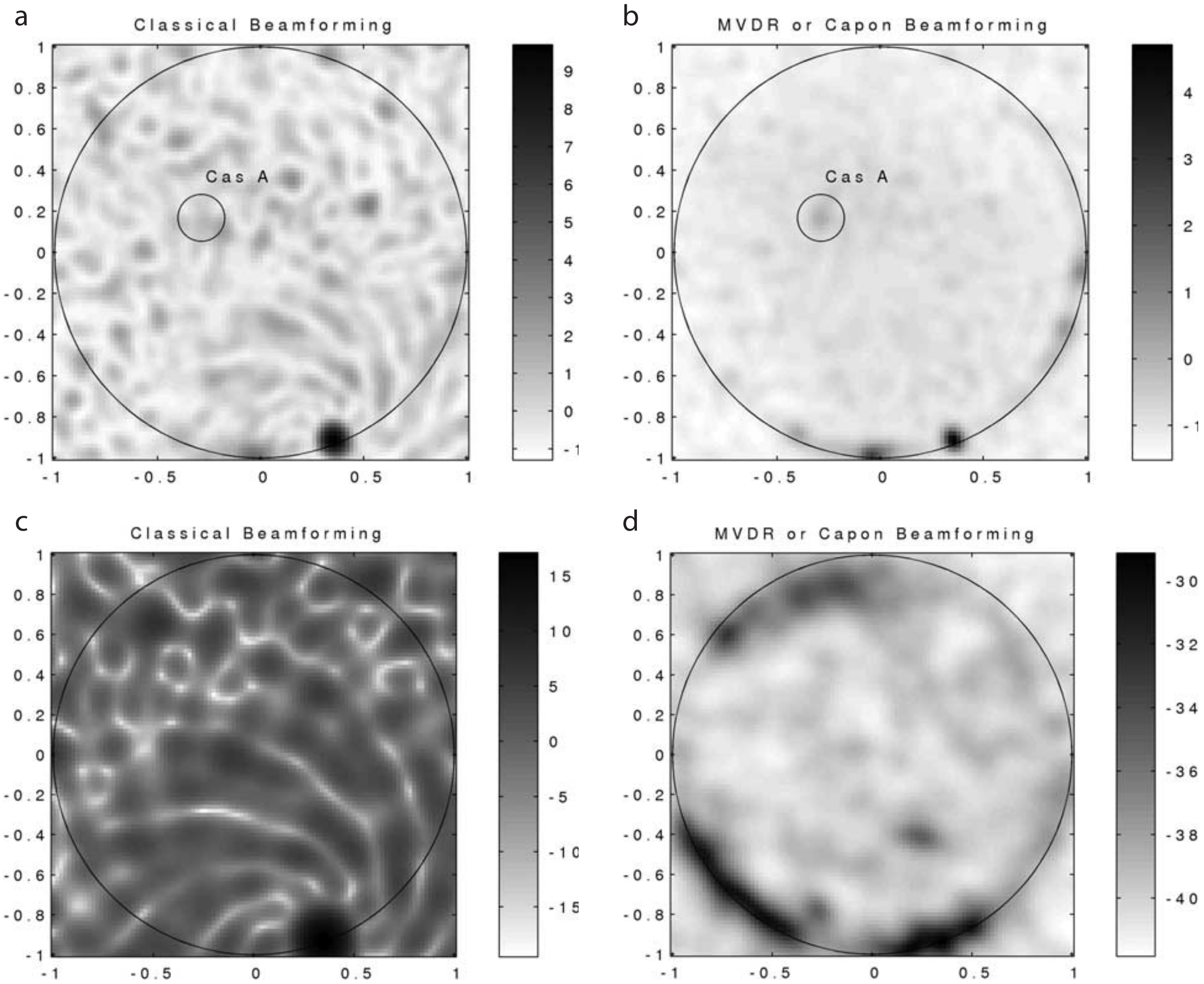

Figure 9. Celestial daytime maps obtained with the LOFAR test station using the MVDR beam former and the classical beam former. (a–b) Shown are Cas.A and a transmitter at the horizon at 11.86 MHz and 9.77 kHz bandwidth. (c–d) Shown are the same results, but at a nearby frequency with a more dominant transmitter.

gain. More robust versions of MVDR exist such as robust capon beam forming [*Stoica et al.*, 2003], but these are not discussed in detail here.

[53] Spatially filtered data in the sky maps can be corrected using space varying beams [*Leshem et al.*, 2000]. MVDR and robust capon beam formers can be extended to include such operations. Figure 9 shows illustrations of the use of a classical beam former and an MVDR beam former to produce "dirty" images. The top images show that an MVDR beam former has a much sharper beam than compared to the classical beam former, and a much smoother sidelobe structure. In this daytime observation, the classical beam former does not reveal the strong source Cas.A; the MVDR beam former does show the source. A drawback of MVDR is that calibration errors can cause the MVDR beam former to underestimate the power. Especially the higher peaks can be strongly diminished by this effect, resulting in a lower dynamic range. A clear example of this effect is shown in Figures 9c and 9d. The difference in dynamic range is more than 20 dB. In literature, methods have been proposed to improve the performance of the MVDR beam former for arrays with imperfect calibration. We have chosen the robust capon beam forming method of

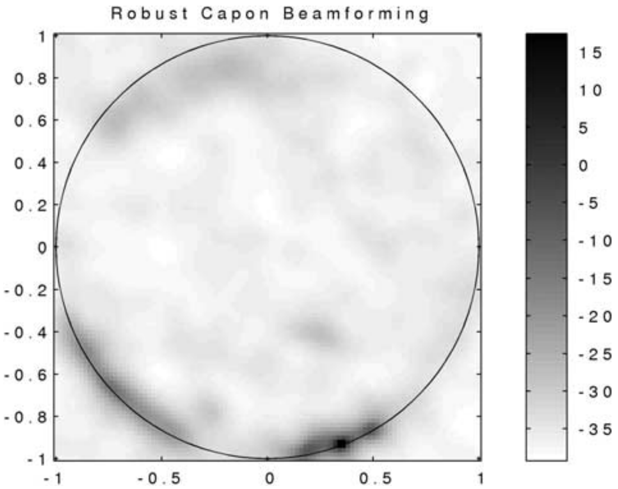

Figure 10. Celestial map obtained with the LOFAR test station using the robust capon beam former. The image shows the sky at 11.86 MHz and at a bandwidth of 9.77 kHz. A strong interfering source is visible at the bottom right horizon; a band of interfering signals is visible at the bottom left horizon. Cas.A and the galactic plane are not visible.

Li, Stoica, and Wang as proposed by *Stoica et al.* [2003]. The result of this method is shown in Figure 10. The intensity scaling (array/beam gain) is restored. The observed beam width is very small, which suggests that robust capon beam forming could enhance some of the calibration approaches in the astronomical imaging process. This, however, needs further study.

5. Conclusions

[54] In this paper we have demonstrated spatial filtering capabilities at the LOFAR initial test station (ITS), and have related it to the LOFAR RFI mitigation strategy. We have shown that with ITS, in frequency ranges which are occupied with moderate-intensity interfering signals, the strongest astronomical sky sources can be recovered by spatial filtering. The same Selfcal and Clean approaches which remove the sidelobe structures of the strongest sources such as Cas.A can also be used to mitigate the interference further. The spatial dilution effect helps reducing the interference. We have also shown that intermodulation products originating from point sources remain point sources and can be attenuated with the same spatial filtering techniques as nonintermodulation interference. We have shown and verified experimentally that even the direction of an intermodulation product can be predicted. Finally, we have demonstrated the use of several beam former types for ITS.

References

Barnbaum, C., and R. F. Bradley (1998), A new approach to interference excision in radio astronomy: Real-time adaptive cancellation, *Astron. J.*, *115*, 2598–2614.

Boonstra, A. J. (2002), RFI mitigation strategy, *Rep. LOFAR-ASTRON-DOC-004*, Low Frequency Array, Dwingeloo, Netherlands.

Boonstra, A. J., and A. J. van der Veen (2003a), Dual polarization gain estimation for radio telescope arrays, paper presented at IEEE International Conference on Acoustics, Speech, and Signal Processing (ICASSP), Inst. of Electr. and Electron. Eng., Hong Kong, April.

Boonstra, A. J., and A. J. van der Veen (2003b), Gain calibration methods for radio telescope arrays, *IEEE Trans. Signal Process.*, *51*(1), 25–38.

Bregman, J. D. (2000), Concept design for a low frequency array, in *Radio Telescopes*, *Proc. SPIE*, vol. 4015, edited by H. R. Butcher, pp. 19–32, Int. Soc. for Opt. Eng., Bellingham, Wash.

Briggs, F. H., J. F. Bell, and M. J. Kesteven (2000), Removing radio interference from contaminated astronomical spectra using an independent reference signal and closure relations, *Astron. J.*, *120*, 3351–3361.

Ellingson, S. W., J. D. Bunton, and J. F. Bell (2001), Removal of the GLONASS C/A signal from OH spectral line observations using a parametric modelling technique, *Astrophys. J. Suppl. Ser.*, *135*(1), 87–93.

Fridman, P. A., and W. A. Baan (2001), RFI mitigation methods in radio astronomy, *Astron. Astrophys.*, *378*, 327–344.

International Telecommunication Union (2003), Protection criteria used for radio astronomical measurements, in *Recommendation ITU-R RA.769-1*, Geneva, Switzerland.

Kollen, H. (2004), LOFAR system requirements specification, *Rep. LOFAR-ASTRON-SRS-001*, Low Frequency Array, Dwingeloo, Netherlands, May.

Kraus, J. D. (1986), *Radio Astronomy*, 2nd ed., McGraw-Hill, New York.

Leshem, A., and A. J. van der Veen (2000), The effect of adaptive interference suppression on radio astronomical image formation, in *Radio Telescopes*, *Proc. SPIE*, vol. 4015, edited by H. R. Butcher, pp. 341–352, Int. Soc. for Opt. Eng., Bellingham, Wash.

Leshem, A., A. J. van der Veen, and A. J. Boonstra (2000), Multichannel interference mitigation techniques in radio astronomy, *Astrophys. J. Suppl. Ser.*, *131*(1), 355–373.

Madisetti, V. K., and D. B. Williams (Eds.) (1998), *The Digital Signal Processing Handbook*, *Electr. Eng. Handbook Ser.*, CRC Press, Boca Raton, Fla.

Mardia, K. V., J. T. Kent, and J. M. Bibby (1979), *Multivariate Analysis*, *Probab. Math. Stat.*, Elsevier, New York.

Noordam, J. E. N. (2002), Generalized self-calibrattion for LOFAR, paper presented at 27th General Assembly of the International Union of Radio Science, Maastricht, Netherlands, Aug.

Noordam, J. E. N. (2004), LOFAR calibration challenges, paper presented at SPIE Conference on Astronomical Telescopes and Instrumentation, Int. Soc. for Opt. Eng., Glasgow, U. K., June.

Perley, R. A., F. R. Schwab, and A. H. Bridle (1994), *Synthesis Imaging in Radio Astronomy*, *Astron. Soc. Pac. Conf. Ser.*, vol. 6, Astron. Soc. of the Pac., San Francisco, Calif.

Raimond, E., and R. Genee (Eds.) (1996), *The Westerbork Observatory, Continuing Adventure in Radio Astronomy*, *Astrophys. Space Libr.*, vol. 207, Springer, New York.

Raza, J., A. J. Boonstra, and A. J. van der Veen (2002), Spatial filtering of RF interference in radio astronomy, *IEEE Signal Process. Lett.*, *9*, 64–67.

Rohlfs, K. (1990), *Tools of Radio Astronomy*, Springer, New York.

Stoica, P., Z. Wang, and J. Li (2003), Robust capon beamforming, *IEEE Signal Process. Lett.*, *10*, 172–175.

Thompson, A. R., J. R. Moran, and G. W. Swenson (1986), *Interferometry and Synthesis in Radio Astronomy*, 1st ed., John Wiley, Hoboken, N. J.

van der Tol, S. V., and A. J. van der Veen (2004), Performance analysis of spatial filtering of RF interference in radio astronomy, *IEEE Trans. Signal Process.*, *53*, 896–910.

Van Trees, H. L. (2002), *Detection, Estimation, and Modulation Theory*, part 4, *Optimum Array Processing*, Wiley-Interscience, Hoboken, N. J.

Whalen, A. D. (1971), *Detection of Signals in Noise*, Elsevier, New York.

Wijnholds, S. J., J. D. Bregman, and A. J. Boonstra (2005), Sky noise limited snapshot imaging in the presence of RFI with the LOFAR initial test station, *Exp. Astron.*, in press.

A. J. Boonstra, Research and Development Department, ASTRON, Oude Hoogeveensedijk 4, NL-7991 PD Dwingeloo, Netherlands. (boonstra@astron.nl)

S. van der Tol, Department of Electrical Engineering, Delft University of Technology, Mekelweg 4, NL-2628 CD Delft, Netherlands. (svdt@cas.et.tudelft.nl)